



HAL
open science

A relation between lava discharge rate, thermal insulation, and flow area set using lidar data

Andrew J.L. J.L. Harris, Massimiliano Favalli, A. Steffke, Alessandro Fornaciai, E. Boschi

► To cite this version:

Andrew J.L. J.L. Harris, Massimiliano Favalli, A. Steffke, Alessandro Fornaciai, E. Boschi. A relation between lava discharge rate, thermal insulation, and flow area set using lidar data. *Geophysical Research Letters*, 2010, 37, pp.L20308. 10.1029/2010GL044683 . hal-00576118

HAL Id: hal-00576118

<https://hal.science/hal-00576118>

Submitted on 19 Oct 2021

HAL is a multi-disciplinary open access archive for the deposit and dissemination of scientific research documents, whether they are published or not. The documents may come from teaching and research institutions in France or abroad, or from public or private research centers.

L'archive ouverte pluridisciplinaire **HAL**, est destinée au dépôt et à la diffusion de documents scientifiques de niveau recherche, publiés ou non, émanant des établissements d'enseignement et de recherche français ou étrangers, des laboratoires publics ou privés.

Copyright

A relation between lava discharge rate, thermal insulation, and flow area set using lidar data

Andrew Harris,¹ Massimiliano Favalli,² Andrea Steffke,³ Alessandro Fornaciai,² and Enzo Boschi²

Received 14 July 2010; accepted 27 August 2010; published 22 October 2010.

[1] A simple linear relation can be used to link time averaged discharge rate (TADR) and lava flow area (A). The relation applies to given insulation conditions, as described by the characteristic flow surface temperature (T_e), and will vary from case-to-case depending on rheological and topographic influences on flow spreading. Most flows have insulation conditions that change through time, modifying the relationship between TADR and area as insulation conditions evolve. Using lidar data we can define TADR, the flow area that the discharge feeds and T_e , allowing generation of a case-specific relation to convert satellite-data-derived flow areas to TADR. For Etna's 2006 lava flow field we obtain a relation whereby $TADR = 5.6 \times 10^{-6} A$ for well insulated conditions ($T_e = 100^\circ\text{C}$) and $TADR = 1.5 \times 10^{-4} A$ for poorly insulated conditions ($T_e = 600^\circ\text{C}$). **Citation:** Harris, A., M. Favalli, A. Steffke, A. Fornaciai, and E. Boschi (2010), A relation between lava discharge rate, thermal insulation, and flow area set using lidar data, *Geophys. Res. Lett.*, 37, L20308, doi:10.1029/2010GL044683.

1. Introduction

[2] Lava flow dimensions have been used to define empirical relationships between lava volume flux and flow length [Walker, 1973], volume [Malin, 1980] and area [Pieri and Baloga, 1986]. Volume fluxes used to define these relations use time-averaged values, usually obtained by taking the lava volume emplaced during a known time period and dividing by that time to give a time-averaged discharge rate (TADR). Correlations also involve data for individual flow units emplaced under specific thermal, rheological and topographic conditions, and should only be applied to those conditions for which they were derived [e.g., Pinkerton and Wilson, 1994]. The relation of Pieri and Baloga [1986] was subsequently adapted to convert satellite thermal data to TADR [Harris et al., 1997], and has been argued to reduce to a simple empirical relation [Wright et al., 2001] which must be set depending on appropriate insulation, rheological and topographic conditions [Harris and Baloga, 2009]. Although simultaneously-acquired TADR and flow area data allow these relations to be set, suitable topographic data have been lacking. Recent availability of lidar data and improved photogrammetric techniques now provide suitable data. For active lava flows, such data now exist for Etna's 2001 [Cottelli et al., 2007], 2004 [Mazzarini et al., 2005]

and 2006 [Favalli et al., 2010] lava flows, plus Stromboli's 2007 flows [Marsella et al., 2009]. We use these data to explore an empirical relation between TADR and active flow area for these eruptions.

2. Time-Averaged Discharge Rate and Lava Flow Plan Area: Thermal Controls

[3] Pieri and Baloga [1986] proposed an empirical relation between TADR and active lava flow area (A), the physical basis of which was that heat losses caused the flow to cool with distance from the vent so that spreading ceased once the flow cooled through a critical temperature range (ΔT):

$$TADR = A \frac{\varepsilon\sigma(T_e^4 - T_a^4) + h_c(T_e - T_a)}{\rho(c_p\Delta T + L\Delta\phi)} \quad (1)$$

All variables and constants are defined in Table 1. The result is a discharge rate time-averaged over the period required for lava to spread over area A and/or to cool by ΔT [Wright et al., 2001]. Given the assumptions involved, the relation reduces to $TADR = mA/c$, m being $\varepsilon\sigma(T_e^4 - T_a^4) + h_c(T_e - T_a)$ and c being $\rho(c_p\Delta T + L\Delta\phi)$ [Harris et al., 2007]. That is, we expect a good correlation between flow area and heat flux, and hence also volume flux [Wright et al., 2001]. For any rheological or topographic case the main variables thus become active flow area and characteristic surface temperature, as described by the effective radiation temperature (T_e). Thus, given appropriate cooling and crystallization conditions (e.g., Table 1), a linear relation between TADR and A can be plotted for each T_e (Figure 1). For any T_e , increased TADR should result in increased active flow area. T_e is also a measure of flow insulation: the lower the T_e , the greater the degree of insulation. Insulation reduces heat losses and core cooling rates. Consequently, as insulation increases, so too should the area that a lava flow can cover before solidifying.

[4] A relation has to be derived for each insulation case. While use of $T_e = 1000^\circ\text{C}$ may describe a relation for a poorly insulated flow, $T_e = 100^\circ\text{C}$ may apply to a well insulated flow. Within the Figure 1 framework, we can now move in three possible directions. If overall insulation conditions remain constant, so that area increases linearly with TADR, we move up or down any given T_e line (Trend 1). If, instead, TADR remains constant and insulation conditions change, we move horizontally across the graph moving from one T_e line to another as insulation conditions evolve, so that area increases with decreasing T_e (Trend 2). Finally, if TADR and insulation conditions change, area increases with TADR, but the trend is modified by changing insulation

¹Laboratoire Magmas et Volcans, Université Blaise Pascal, Clermont-Ferrand, France.

²Istituto Nazionale di Geofisica e Vulcanologia, Pisa, Italy.

³HIGP, SOEST, University of Hawai'i, Honolulu, Hawaii, USA.

Table 1. Values Used to Derive a Relation Between TADR and Lava Flow Area for Etna’s 2006 Flow Field and the Relation These Yield

Symbol	Definition	Model 1	Model 2	Model 3	Model 4	Units	Source
T_c	Characteristic surface temperature	100–600	100–600	100–600	100–600	°C	Typical range of data plotted in Figure 1
ϵ	Lava emissivity	0.9887	0.9887	0.9887	0.9887		Basalt emissivity [Salisbury and D’Aria, 1992]
σ	Stefan-Boltzmann constant	5.67×10^{-8}	5.67×10^{-8}	5.67×10^{-8}	5.67×10^{-8}	$W m^{-2} K^{-4}$	
T_a	Ambient temperature	25	25	25	25	°C	
h_c	Convective heat transfer coefficient	10	10	10	10	$W m^{-2} K^{-1}$	Calculated from Holman [1992]
ρ_{DRE}	Dense Rock Density	2700	2700	2700	2700	$kg m^{-3}$	Method of Bottinga and Weill [1970] with the chemistry for Etna given by Pompilio et al. [1998] and Taddeucci et al. [2004]
c_{pDRE}	Specific heat capacity	1130	1130	1130	1130	$J kg^{-1} K^{-1}$	Calculated for a temperature of 1100°C following Keszthelyi [1994]
ϖ	Vesicularity	0.22	0.22	0.55	0.55	fraction	Mean value from data given by Herd and Pinkerton [1997] and Gaonac’h et al. [1996], and best-fit value of Figure 2c–2d
ρ	Density (bulk-rock)	2106	2106	1215	1215	$kg m^{-3}$	$= \rho_{DRE} \times (1 - \varpi)$
c_p	Specific heat capacity (bulk-rock)	881	881	509	509	$J kg^{-1} K^{-1}$	$= c_{pDRE} \times (1 - \varpi)$
ΔT	Lava cooling between eruption temperature and temperature at which flow is no longer possible	100	50	100	200	°C	Best-fit values of Figure 2
L	Latent Heat of crystallization	3.5×10^5	3.5×10^5	3.5×10^5	3.5×10^5	$J kg^{-1} K^{-1}$	
$\Delta\varphi$	Crystallization in cooling through ΔT	0.1	0.2	0.45	0.3	fraction	Best-fit values of Figure 2
<i>Coefficients for Linear Best-Fit (TADR = x A)</i>							
m	$T_c = 100^\circ C$ condition	1.4	1.4	1.4	1.4	$\times 10^3 W m^{-2}$	$m = \epsilon\sigma(T_c^4 - T_a^4) + h_c(T_c - T_a)$
	$T_c = 600^\circ C$ condition	3.8	3.8	3.8	3.8	$\times 10^4 W m^{-2}$	$m = \epsilon\sigma(T_c^4 - T_a^4) + h_c(T_c - T_a)$
c	All T_c conditions	2.6	2.4	2.5	2.5	$\times 10^8 J m^{-3}$	$c = \rho(c_p\Delta T + L\Delta\varphi)$
x	$T_c = 100^\circ C$ condition	5.4	5.8	5.5	5.6	$\times 10^{-6} m s^{-1}$	$x = m/c$, so that TADR = x A
	$T_c = 600^\circ C$ condition	1.5	1.6	1.5	1.5	$\times 10^{-4} m s^{-1}$	$x = m/c$, so that TADR = x A

conditions. In such cases, area changes with TADR but does not follow any single T_c line. Instead, we move across the T_c lines (Trend 3a). If we move in a perfectly vertical direction, the insulation effect is balancing the TADR effect, so that the active flow area does not change with TADR (Trend 3b).

If the insulation effect outweighs the TADR effect, flow area can actually increase with declining TADR (Trend 3c).

[5] We can now plot flow area and TADR data within the Figure 1 framework to assess the insulation conditions associated with given lava flow emplacement events. If insu-

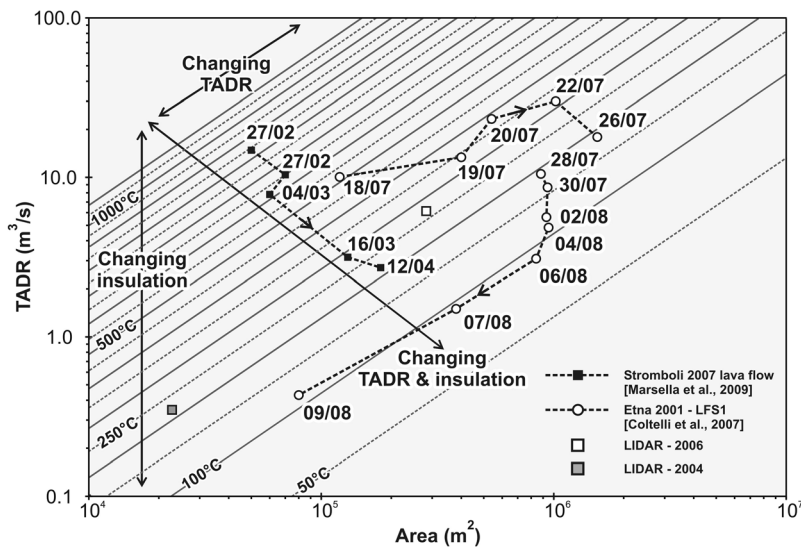


Figure 1. TADR versus lava area relations plotted for Etna using the values of Table 1. Relations are plotted in 50°C increments between T_c of 50°C and 1100°C. Main trends that changes in TADR and/or insulation can cause in the evolution of a lava flow area through time are marked, and available data for Etna and Stromboli are overplotted.

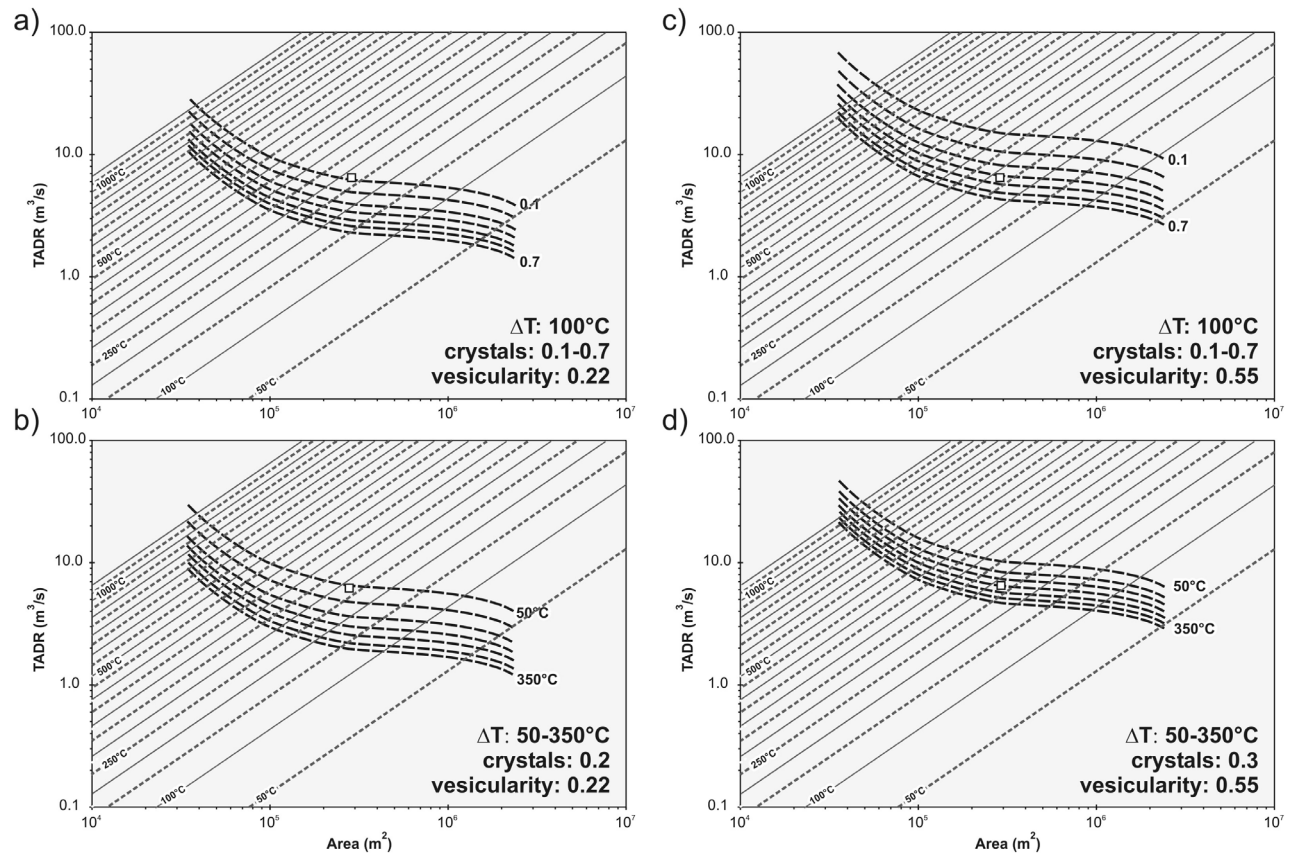


Figure 2. TADR versus lava area relations of Figure 1 with the data point provided by our 17–18 November 2006 lidar data (black square). Each curve represents the solution range for active area and TADR estimates made using an AVHRR image acquired on 17 November 2006 with T_e ranging from 100°C to 1000°C. (a) The solution curves for vesicularity = 0.22, $\Delta T = 100^\circ\text{C}$ and $\Delta\varphi$ in the range 0.1 to 0.7 (in increments of 0.1 between these end points). (b) The solution curves for vesicularity = 0.22, $\Delta\varphi = 0.2$ and ΔT in the range 50°C to 350°C (in increments of 50°C between these end points). (c) The solution curves for vesicularity = 0.55, $\Delta T = 100^\circ\text{C}$ and $\Delta\varphi$ in the range 0.1 to 0.7. (d) The solution curves for vesicularity = 0.55, $\Delta\varphi = 0.3$ and ΔT in the range 50°C to 350°C.

lation conditions are stable the data should define a linear relation that follows a single T_e line, along which increased TADR results in increased flow area. If data do not plot along such a line, then we can use Figure 1 to assess the evolving insulation conditions. We note, though, that these relations will be modified by topographic (e.g., slope) or rheological (e.g., viscosity) conditions, and break down if lava spreading is inhibited (e.g., if it becomes contained within a pit). If, for example, viscosity increases or slope decreases, the ability of the lava to spread will be reduced and a new relation will have to be defined. Thus, as has been done to date, relations have to be set case-by-case to fit appropriate insulation, rheological and topographic conditions [Harris and Baloga, 2009].

[6] The relation found to provide a best-fit between TADR and flow area at Etna and Stromboli is used for Figure 1 (as given in Table 1). Over this we plot available topographic-data-derived TADR and flow areas for these two volcanoes. Data for Stromboli's 2007 lava flows given by Marsella *et al.* [2009] show a trend of increasing area with decreased TADR (Figure 1). This Type 3c trend develops through time, suggesting that flows were poorly insulated at the onset of the eruption, with insulation improving as the eruption progressed. Insulation was so

effective that flows could extend over increasingly large areas, in spite of declining TADR, a scenario consistent with the development of more heavily crusted flows at lower TADRs. Data for Etna's 2001 lava flows, as given by Coltelli *et al.* [2007], cover two periods: (a) an initial high TADR phase of flow advance, followed by (b) a phase of declining TADR during which flow fronts retreated up the master channel. These data show a Type 3a trend during flow advance, and a Type 1 trend during retreat (Figure 1). The Type 3a trend indicates that flow area increased with TADR, but the trend was modified by evolving insulation conditions, with insulation improving with time to force an up-x-axis movement across the T_e lines of Figure 1. This is consistent with the development of extensive crusted sections on an 'a' flow of steadily increasing length. During this time data points span the $T_e = 500^\circ\text{C}$ to $T_e = 200^\circ\text{C}$ lines (Figure 1). This compares with typical surface temperatures in the range 275 to 380°C estimated for this flow by Lombardo and Buongiorno [2006]. With flow retreat, T_e conditions appear to reach a lower limit, with area decreasing linearly with TADR along the $T_e \approx 100^\circ\text{C}$ line (Figure 1).

[7] Lidar data allow TADR and active flow area to be obtained with some precision, with data being available for flow fields active on Etna in 2004 and 2006 [Favalli *et al.*,

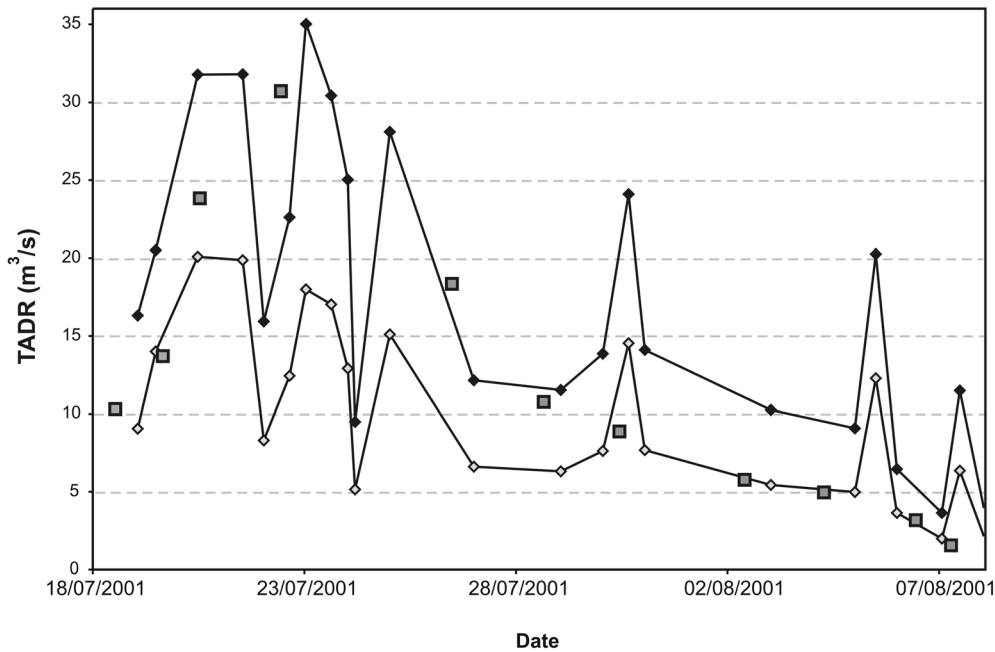


Figure 3. TADR ranges estimated from AVHRR data for lava flow LSF1 active during Etna’s 2001 eruption using the relation given here for Etna in Table 1. Gray squares locate data points obtained by *Coltelli et al.* [2007] using photogrammetry and DEM subtraction.

2009, 2010]. DEM subtraction for the 2006 data indicate a lava volume of $568,110 \pm 2690 \text{ m}^3$ emplaced over $282,745 \text{ m}^2$ in the 25 h period between 09:04Z on 17 November and 10:04Z on 18 November, giving a TADR of $6.31 \pm 0.03 \text{ m}^3 \text{ s}^{-1}$. The 2004 data allow us to estimate the volume for a 915 m long unit active on the southern edge of the flow field. For this flow we obtain a volume of $1620 \pm 360 \text{ m}^3$ emplaced over $22,800 \text{ m}^2$ during 76 minutes on 16 September, giving a TADR of $0.36 \pm 0.08 \text{ m}^3 \text{ s}^{-1}$. Plotting these points on Figure 1 indicates characteristic T_c of 250°C (for the 2006 flow) and 200°C (for the 2004 flow). The latter value compares with a bi-modal distribution of surface temperatures, with modes at $100\text{--}150^\circ\text{C}$ and $250\text{--}300^\circ\text{C}$, obtained for the 16 September 2004 flow by *Wright et al.* [2010]. The relative position of the 2006 and 2004 data points match with the 2006 activity being characterized by channels feeding actively advancing flow fronts, whereas activity at the 2004 unit was dying out, the channel feeding a barely moving flow front. The direction of the trend between the two points mimics that obtained for the waning phase the 2001 flow, and thus characterizes waning activity. We can now use these data to set a relation to extract TADR from satellite derived flow area.

3. A Relation to Allow Satellite-Based TADR Estimates

[8] Application of a simple mixture model to thermal infrared satellite data (TIR, $10\text{--}12 \mu\text{m}$) can be used to estimate the active lava area within pixel x (A_x):

$$A_x = \frac{R_{TIR} - L_{TIR}(T_a)}{L_{TIR}(T_c) - L_{TIR}(T_a)} A_{\text{pixel}} \quad (2)$$

Here, R_{TIR} is the pixel integrated spectral radiance, L_{TIR} is the Planck function, T_c is lava crust temperature, T_a is the temperature of ambient surfaces surrounding the flow and A_{pixel} is pixel area. Summing A_x for all pixels gives total area at T_c . Given a measure of T_a from surrounding (non-lava containing) pixels, solution of equation (2) requires assumption of T_c . Given that we cannot fix a single temperature to characterize T_c , the most reasonable solution is to solve equation (2) across a range of possible T_c [*Harris et al.*, 1997]. End member T_c , and the areas that these give, have thus been used in equation (1) to obtain two end member estimates for TADR within which the actual value usually lies [*Harris et al.*, 2007]. However, plotting the solution range within the Figure 1 framework reveals that the solution range is actually defined by a curve which crosses the T_c lines (Figure 2).

[9] In solving equation (1) we have no constraint on (i) the cooling experienced by the flow (ΔT), (ii) the amount of crystallization in cooling through ΔT ($\Delta\varphi$) or (iii) vesicularity, which will influence the values of density and specific heat capacity (see Table 1). To help resolve this, we plot families of solution curves derived either by (i) holding ΔT constant and varying $\Delta\varphi$ (Figure 2a) or (ii) holding ΔT constant and varying $\Delta\varphi$ (Figure 2b). By assessing the location of each solution curve in relation to the lidar-derived “ground-truth” point for Etna’s 2006 lava flow (Figure 2), we can choose appropriate coefficients to use in an empirical relation between TADR and A . We first see that the lidar-derived point is located where our solution curves intersect the $T_c = 250^\circ\text{C}$ line, indicating this as the likely T_c for this case. There are now infinite parameter combinations that satisfy equation (1). If, for example, we use a vesicularity of 0.22, the average value for Etnean lava’s, we obtain a solution curve which passes through the lidar-derived data point with (i) $\Delta T = 100^\circ\text{C}$ and $\Delta\varphi = 0.1$ (Figure 2a), or

Table 2. Cloud-Free Advanced Very High Resolution Radiometer Images Acquired During 17–18 November 2006, the Active Flow Areas That These Give, and the TADR Obtained Using the Table 1 Conversion^a

Image Date ^b	Area (km ²)			TADR (m ³ s ⁻¹)		
	T = 100°C	T = 250°C	T = 600°C	T = 100°C	T = 250°C	T = 600°C
17 November 2006 (01:07Z)	0.9873	0.2726	0.0780	5.3	6.3	11.4
17 November 2006 (20:46Z)	0.9664	0.2670	0.0764	5.2	6.2	11.2
18 November 2006 (20:33Z)	1.0828	0.2936	0.0836	5.8	6.8	12.2

^aThe lidar derived active area and TADR from DEM subtraction of the 18/11(10:04Z) and 17/11 (09:04Z) images was 0.2827 km² and 6.31 ± 0.03 m³ s⁻¹.

^bTime is in parentheses.

(ii) $\Delta T = 50^\circ\text{C}$ and $\Delta\varphi = 0.2$ (Figure 2b). Using MELTS of Ghiorso and Sack (1995), with the compositions for Etna's lava upon eruption given by Pompilio *et al.* [1998] and Taddeucci *et al.* [2004], if we cool by 100°C from an eruption temperature of $1075 \pm 5^\circ\text{C}$ we obtain $\Delta\varphi$ between 0.16 and 0.46. Thus values of 0.1 to 0.2 seem a little low. However, we can also obtain a fit with the lidar data if we increase vesicularity to 0.55. Other fits are thus attained at $\Delta T = 100^\circ\text{C}$, $\Delta\varphi = 0.45$ (Figure 2c) and $\Delta T = 200^\circ\text{C}$, $\Delta\varphi = 0.3$ (Figure 2d). Our results may indicate that the vesicularity of the 2006 flow was high. However, the degree to which we can alter any of the three variables (ΔT , $\Delta\varphi$, and vesicularity) to obtain a best fit between TADR and area suggests that all we have done is calibrate a linear relation appropriate for this flow. For any given T_e the relation will reduce to $TADR = xA$, in which coefficient x (= m/c) needs to be set for appropriate insulation, cooling, crystallization, rheological and topographic conditions. For the 2006 case we have obtained a fit with the lidar data using $T_e = 250^\circ\text{C}$ and various combinations ΔT , $\Delta\varphi$, and vesicularity. However, each combination yields the same relation, this being defined by x of $\sim 2.4 \times 10^{-5} \text{ m s}^{-1}$. Note that this relation applies to the $T_e = 250^\circ\text{C}$ condition. The relation can, though, be calculated for any other T_e as done in Table 1. In effect, all we have done is adjust our unknowns in equation (1) to achieve a best-fit with available field data, thereby defining a linear relation between TADR and active lava flow area for this 2006 case. This best fit can be achieved with infinite choices of the unknowns in equation (1), where we have chosen reasonable values to derive an empirical best-fit with a linear form.

[10] Testing whether this relation is appropriate to other cases requires knowledge of characteristic T_e . TADR-area data points plotted in Figure 1 indicate T_e typically between 100°C and 600°C for the three Etna eruptions considered here. If we use this range to calculate the limits of the relation we obtain x of $5.6 \times 10^{-6} \text{ m s}^{-1}$ for $T_e = 100^\circ\text{C}$, and 1.5×10^{-4} for $T_e = 600^\circ\text{C}$ (Table 1). Applying these relations to satellite data for Etna's 2001 eruption yield TADR envelopes that are in good agreement with field data (Figure 3), suggesting that this relation is also appropriate for this case. Application of the relation to satellite data for Etna's 2006 eruption also yields good results. Our lidar data for 18 November 2006 give a TADR of $6.31 \pm 0.03 \text{ m}^3 \text{ s}^{-1}$ (averaged over the previous 24 h). Three cloud-free satellite images were acquired over this period (Table 2). All three give roughly same lava area which convert to TADRs between $5.2 \text{ m}^3 \text{ s}^{-1}$ and $12.2 \text{ m}^3 \text{ s}^{-1}$, with an uncertainty $\pm 36\%$. The solution envelopes given in Figure 3 and Table 2 embrace our range of uncertainty, but are sufficiently narrow to allow changes in TADR to be identified and used for

hazard monitoring and assessments of the volcanic processes that drive the changes.

4. Conclusions

[11] Pieri and Baloga [1986] provide a framework within which theoretical relationships between TADR, lava flow insulation and area can be plotted. This framework allows use of lidar-derived TADR and area to assess the thermal state of the flow surface. When applied to satellite data, the relation reduces to a linear best-fit which must be set according to the insulation, cooling, crystallization, rheological and topographic conditions under which the flow was emplaced. If calibrated correctly, the relation provides a simple means to convert satellite-derived lava flow areas to TADR. lidar data for active flow units provides one means of achieving this calibration.

[12] **Acknowledgments.** We thank Matthew Partick and Jon Dehn for their review comments and suggestions. These greatly improved the focus and content of this manuscript. Andrea Steffke was supported by a grant from NASA and the ASTER Science Team (NNX08AJ91G). Alessandro Fornaciai received support from the MIUR-FIRB project "Piattaforma di ricerca multidisciplinare su terremoti e vulcani (AIRPLANE)" n. RBPR05B2ZJ (Italy).

References

- Bottinga, Y., and D. F. Weill (1970), Densities of liquid silicate systems calculated from partial molar volumes of oxide components, *Am. J. Sci.*, 269, 169–182, doi:10.2475/ajs.269.2.169.
- Coltelli, M., C. Proietti, S. Branca, M. Marsella, D. Andronico, and L. Lodato (2007), Analysis of the 2001 lava flow eruption of Mt. Etna from three-dimensional mapping, *J. Geophys. Res.*, 112, F02029, doi:10.1029/2006JF000598.
- Favalli, M., A. Fornaciai, and M. T. Pareschi (2009), Lidar strip adjustment: Application to volcanic areas, *Geomorphology*, 111, 123–135, doi:10.1016/j.geomorph.2009.04.010.
- Favalli, M., A. Fornaciai, F. Mazzarini, A. Harris, M. Neri, B. Behncke, M. Pareschi, S. Tarquini, and E. Boschi (2010), Evolution of an active lava flow field using a multitemporal lidar acquisition, *J. Geophys. Res.*, doi:10.1029/2010JB007463, in press.
- Gaonac'h, H., J. Stix, and S. Lovejoy (1996), Scaling effects on vesicle shape, size and heterogeneity of lavas from Mount Etna, *J. Volcanol. Geotherm. Res.*, 74, 131–153, doi:10.1016/S0377-0273(96)00045-5.
- Ghiorso, M. S., and R. O. Sack (1995), Chemical mass transfer in magmatic processes, IV, A revised and internally consistent thermodynamic model for the interpolation and extrapolation of liquid-solid equilibria in magmatic systems at elevated temperatures and pressures, *Contrib. Mineral. Petrol.*, 119, 197–212, doi:10.1007/BF00307281.
- Harris, A. J. L., and S. M. Baloga (2009), Lava discharge rates from satellite-measured heat flux, *Geophys. Res. Lett.*, 36, L19302, doi:10.1029/2009GL039717.
- Harris, A. J. L., S. Blake, D. A. Rothery, and N. F. Stevens (1997), A chronology of the 1991 to 1993 Etna eruption using AVHRR data: implications for real time thermal volcano monitoring, *J. Geophys. Res.*, 102(B4), 7985–8003, doi:10.1029/96JB03388.

- Harris, A. J. L., J. Dehn, and S. Calvari (2007), Lava effusion rate definition and measurement: A review, *Bull. Volcanol.*, *70*, 1–22, doi:10.1007/s00445-007-0120-y.
- Herd, R. A., and H. Pinkerton (1997), Bubble coalescence in basaltic lava: Its impact on the evolution of bubble populations, *J. Volcanol. Geotherm. Res.*, *75*, 137–157, doi:10.1016/S0377-0273(96)00039-X.
- Holman, J. P. (1992), *Heat Transfer*, 713 pp., McGraw-Hill, London.
- Keszthelyi, L. (1994), Calculated effect of vesicles on the thermal properties of basaltic lava, *J. Volcanol. Geotherm. Res.*, *63*, 257–266, doi:10.1016/0377-0273(94)90078-7.
- Lombardo, V., and M. F. Buongiorno (2006), Lava flow thermal analysis using three infrared bands of remote-sensing imagery: A case study from Mount Etna 2001 eruption, *Remote Sens. Environ.*, *101*, 141–149, doi:10.1016/j.rse.2005.12.008.
- Malin, M. C. (1980), Lengths of Hawaiian lava flows, *Geology*, *8*, 306–308, doi:10.1130/0091-7613(1980)8<306:LOHLF>2.0.CO;2.
- Marsella, M., C. Proietti, A. Sonnessa, M. Coltelli, P. Tommasi, and E. Bernardo (2009), The evolution of the Sciara del Fuoco subaerial slope during the 2007 Stromboli eruption: Relation between deformation processes and effusive activity, *J. Volcanol. Geotherm. Res.*, *182*, 201–213, doi:10.1016/j.jvolgeores.2009.02.002.
- Mazzarini, F., M. T. Pareschi, M. Favalli, I. Isola, S. Tarquini, and E. Boschi (2005), Morphology of basaltic lava channels during the Mt. Etna September 2004 eruption from airborne laser altimeter data, *Geophys. Res. Lett.*, *32*, L04305, doi:10.1029/2004GL021815.
- Pieri, D. C., and S. M. Baloga (1986), Eruption rate, area, and length relationships for some Hawaiian lava flows, *J. Volcanol. Geotherm. Res.*, *30*, 29–45, doi:10.1016/0377-0273(86)90066-1.
- Pinkerton, H., and L. Wilson (1994), Factors effecting the lengths of channel-fed lava flows, *Bull. Volcanol.*, *56*, 108–120.
- Pompilio, M., R. Trigila, and V. Zanon (1998), Melting experiments on Mt. Etna lavas: I – The calibration of an empirical geothermometer to estimate the eruptive temperature, *Acta Vulcanol.*, *10*(1), 67–75.
- Salisbury, J. W., and D. M. D’Aria (1992), Emissivity of terrestrial materials in the 8–14 μm atmospheric window, *Remote Sens. Environ.*, *42*, 83–106, doi:10.1016/0034-4257(92)90092-X.
- Taddeucci, J., M. Pompilio, and P. Scarlato (2004), Conduit processes during the July–August 2001 explosive activity of Mt. Etna (Italy): Inferences from glass chemistry and crystal size distribution of ash particles, *J. Volcanol. Geotherm. Res.*, *137*, 33–54, doi:10.1016/j.jvolgeores.2004.05.011.
- Walker, G. P. L. (1973), Lengths of lava flows, *Philos. Trans. R. Soc. London, B*, *274*, 107–118.
- Wright, R., S. Blake, A. Harris, and D. Rothery (2001), A simple explanation for the space-based calculation of lava eruptions rates, *Earth Planet. Sci. Lett.*, *192*, 223–233, doi:10.1016/S0012-821X(01)00443-5.
- Wright, R., H. Garbeil, and A. G. Davies (2010), Cooling rate of some active lavas determined using an orbital imaging spectrometer, *J. Geophys. Res.*, *115*, B06205, doi:10.1029/2009JB006536.

E. Boschi, M. Favalli, and A. Fornaciai, Istituto Nazionale di Geofisica e Vulcanologia, via della Faggiola 32, I-56100 Pisa, Italy.

A. Harris, Laboratoire Magmas et Volcans, Université Blaise Pascal, 5 Rue Kessler, 63038 Clermont-Ferrand, France. (a.harris@opgc.univ-bpclermont.fr)

A. Steffke, HIGP, SOEST, University of Hawai’i, 1680 East-West Rd., Honolulu, HI 96822, USA.